Dynamics and Retinal Structural Changes in the Photocycle of the Artificial Bacteriorhodopsin Pigment BR6.9†

G. H. Atkinson,*,# Y. Zhou,#,‡ L. Ujj,#,§ A. Aharoni,⊥ M. Sheves,*,⊥ and M. Ottolenghi*,||

Department of Chemistry and Optical Science Center, University of Arizona, Tucson, Arizona 85721, Department of Organic Chemistry, Weizmann Institute, Rehovot, Israel, Department of Physical Chemistry, Hebrew University, Jerusalem, Israel, and Department of Physics, University of West Florida, Pensacola, Florida 32503

Received: May 17, 2001; In Final Form: October 23, 2001

The molecular mechanism describing the initial 200 ps of the room-temperature photocycle in the artificial bacteriorhodopsin (BR) pigment, BR6.9, is examined by both absorption and vibrational spectroscopy. The BR6.9 pigment contains a structurally modified retinal chromophore (retinal 6.9) having a six-membered carbon ring bridging the C_9═C_{10}−C_{11} bonds. Picosecond transient absorption (PTA) data show that the initial 200-ps interval of the BR6.9 photocycle contains two intermediates: J6.9 formed with a <3-ps time constant and decaying to K6.9 with a 5-ps time constant (K6.9 has a >5-ns lifetime). Resonantly enhanced vibrational spectra from the light- and dark-adapted ground states of BR6.9 are measured using picosecond resonance coherent anti-Stokes Raman scattering (PR/CARS). Each of these PR/CARS spectra (800−1700 cm^{-1}) contains 33 features assignable to the vibrational degrees of freedom in the retinal chromophore. CARS spectra from the K6.9, obtained from picosecond time-resolved CARS (PTR/CARS) data using 10-ps, 50-ps, 100-ps, and 200-ps time delays following the 570-nm initiation of the BR6.9 photocycle, contain a comparable number of features assignable to the retinal in K6.9. The vibrational spectrum of J6.9 can be tentatively characterized by two bands observed in the 1120−1200-cm^{-1} region from the analysis of the 10-ps PTR/CARS data. Comparisons involving these PTA and CARS data from BR6.9, as well as analogous results obtained from the ground states and photocycle intermediates of native BR and other artificial BR pigments, demonstrate that restricting retinal motion at the C_9═C_{10}−C_{11} bonds does not generally change the initial 200-ps photocycle mechanism, but does alter the rates at which specific molecular processes occur. These vibrational CARS spectra show that the retinal structures in K6.9 and in both light- and dark-adapted BR6.9 are all distinct. However, the specific mechanistic role, if any, of C_{13}═C_{14} isomerization cannot be directly identified from CARS data recorded from BR6.9 and its photocycle intermediates. Even though C_{13}═C_{14} isomerization has been widely considered the primary retinal structural change underlying the proton-pumping mechanism in BR pigments, these results leave open the question of whether C_{13}═C_{14} isomerization is required as a mechanistic precursor for biochemical activity in BR pigments such as BR6.9.

Introduction

The purple membrane of the archaebacterium, *Halobacterium salinarium*, has evolved a highly efficient molecular mechanism within its single, transmembrane protein, bacteriorhodopsin (BR), by which to store and efficiently utilize absorbed light energy.[1,2] Biochemically, BR functions as a proton pump that generates a chemical gradient across its cell membrane to energetically drive ATP synthesis and extracellular signal transduction.[3] The versatility with which this molecular mechanism adapts to changes in the physical and chemical environment of the membrane protein while maintaining its protein functionality has long been of interest, but has yet to be well understood quantitatively.

Isomerization of the C_{13}═C_{14} bond (all-*trans* to 13-*cis*) in the retinal chromophore during the room temperature BR photocycle has been widely considered as a primary molecular event necessary for biochemical activity in this protein (for reviews, see refs 4−6), and therefore, this process appears in essentially all mechanistic models describing energy storage and signal transduction in BR.[1−6] Although widely thought to occur early in the mechanism (i.e., prior to the formation of K intermediates), the precise step within the BR photocycle when C═C isomerization occurs has remained unresolved. Recently, PTR/CARS data from the native J-625 intermediate (∼500 fs lifetime) demonstrated that its retinal structure is distinct from those in both BR-570 and K-590.[7] For example, PTR/CARS spectra indicate that the J-625 retinal differs from the retinal in BR-570 by having (i) increased electron density in the C═C stretching modes, (ii) significantly increased delocalized hydrogen out-of-plane (HOOP) motion, and (iii) restrictions in the CH_3 in-plane rocking motion.[7] In addition, the Schiff-base bonding environment of J-625 is similar to that in BR-570, but different from that in K-590.[7] Other differences in the respective vibrational spectra appear for J-625 and K-590.[7] It is important to note, however, that the C−C stretching bands (i.e., fingerprint bands), long regarded as spectroscopic markers for C═C

† Part of the special issue "Misuo Tasumi Festschrift".
* To whom correspondence should be addressed.
# University of Arizona.
‡ Current address: Lightwave Electronics, Mountain View, California.
§ University of West Florida.
⊥ Weizmann Institute.
|| Hebrew University.

10.1021/jp011911d CCC: $22.00
Published on Web 01/12/2002

isomerization in retinal,[2,8−11] are essentially the same for BR-570 and J-625 and significantly different for J-625 and K-590.[7] Thus, C−C stretching bands indicate that BR-570 and J-625 have the same retinal isomeric (C═C bond) configuration (all-*trans*), while J-625 and K-590 have different retinal isomeric configurations. The changes in the J-625 and BR-590 vibrational spectra show that these retinal structures differ with respect to other molecular coordinates within the retinal (e.g., out-of-plane and CH_3 rocking motions) or interactions between the retinal and specific parts of the protein-binding pocket or both.[7]

Normal mode assignments, based on analyses of conventional Raman spectra from artificial BR pigments incorporating retinals containing isotopes selectively substituted at specific bonds, can, in principle, provide bond specific interpretations of vibrational data.[8−10] Of interest here is the appearance of a band near 1196 cm^{-1} that has been used to assign a 13-*cis* retinal isomer to K-590.[8−11] PTR/CARS data confirm the appearance of the 1196 cm^{-1} band for K-590.[12] On the basis of the normal mode assignment of the 1196 cm^{-1}, therefore, PTR/CARS data show that C_{13}═C_{14} isomerization does not occur prior to J-625 formation, but rather as J-625 transforms into K-590.[7] These CARS results are consistent with fluorescence and stimulated emission data from the I-480 intermediate, which precedes J-625 in the native BR photocycle and which is also thought to have an all-*trans* retinal configuration.[13]

Studies of the primary molecular events comprising the photoreactions in artificial BR pigments containing structurally modified retinals offer excellent opportunities to elucidate the relative importance of specific reaction coordinates.[14−18] A variety of artificial BR pigments are available that control or alter specific parts of the retinal bonding so that their influence, if any, on C_{13}═C_{14} isomerization can be selectively determined. Of particular interest here are artificial BR pigments in which the retinal contains a carbon ring that selectively blocks isomerization or rotation or both at particular C═C and/or C−C bonds.[14−18]

The conclusions about C_{13}═C_{14} isomerization in the native BR photocycle are strongly supported by vibrational spectra from the artificial BR pigment BR5.12 (containing a rigid, five-membered carbon ring structure blocking C_{13}═C_{14} isomerization), which does not have a photocycle or any biochemical activity.[15,17] The only intermediate appearing after the excitation of BR5.12, T5.12, has absorption and vibrational (PTR/CARS) spectra that are similar to those of J-625 (i.e., red-shifted absorption spectrum relative to its ground state, BR5.12 and an all-*trans* retinal CARS spectrum[17]). Thus, PTR/CARS shows that an artificial BR intermediate structurally analogous to J-625 can be formed even when C_{13}═C_{14} isomerization is blocked.[17]

These types of vibrational studies indicate that, although C_{13}═C_{14} isomerization may be a structural transformation essential for biochemical activity in BR (i.e., transmembrane proton pumping), it may not be the initial or primary structural event in the retinal chromophore. Other, independent structural changes (e.g., out-of-plane and CH_3 rocking motions), also critical to biochemical activity, may precede C_{13}═C_{14} isomerization or C_{13}═C_{14} isomerization may occur at different stages of a biochemically active BR photocycle, depending on the structural constraints present within the retinal. In this respect, it should be noted that recent results from atomic force sensing (AFS) measurements on BR, as well as light-induced catalyzed reactions, indicate that the protein undergoes light-induced changes that are not due to the chromophore isomerization.[14,15]

In this study, picosecond transient absorption (PTA) and coherent anti-Stokes Raman vibrational scattering (CARS) data

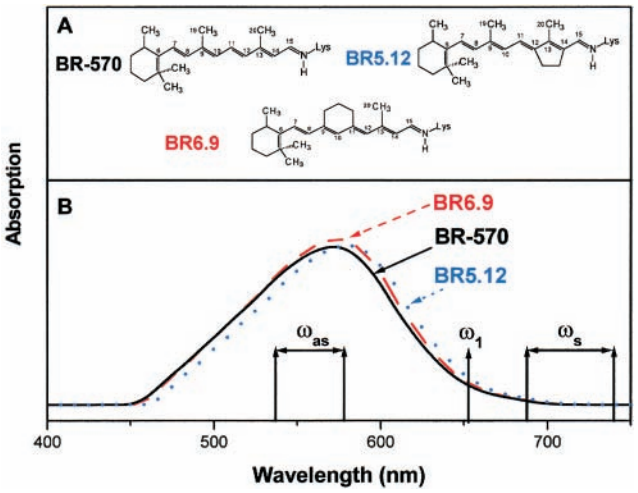

Figure 1. Retinal structures (A) of BR-570, BR5.12, and BR6.9 and (B) the absorption spectra of BR-570 (solid line, maximum at 570 nm), BR5.12 (dotted line, maximum at 578 nm), and BR6.9 (dashed line, maximum at 572 nm). The pump (ω_1 = 663 nm) and probe (ω_s = 685−740 nm) wavelengths used to obtain picosecond resonance coherent anti-Stokes Raman spectra (PR/CARS) from the BR-570 and BR6.9 pigments are shown at the bottom of panel B together with the spectral region (537−575 nm) where the ω_{as} signal appears.

are recorded from the BR6.9 pigment in which a six-membered carbon ring (Figure 1) effectively blocks permanent isomerization and/or rotation in the C_9═C_{10}−C_{11} region, but does not directly prevent C_{13}═C_{14} isomerization. This structural modification in BR6.9, therefore, can be used to determine the influence, if any, on C_{13}═C_{14} isomerization of both (i) increased rigidity in the retinal geometry near the C_9═C_{10}−C_{11} bonds and (ii) restricted isomerization or rotation around the C_9═C_{10}−C_{11} bonds. Independent studies have shown that BR6.9 has a complete photocycle comprised of intermediates apparently analogous to those in wild-type, native BR and pumps protons.[18,19]

The intermediates appearing during the initial (<100 ps) time interval of the native BR photocycle have been identified by femto/picosecond transient absorption (FTA/PTA) spectroscopy: I-460 (<50-fs rise and <200−500-fs decay times)[19−21] and J-625 (<500-fs rise and 3.5-ps decay time)[22] in the native BR photocycle are identified respectively from 460-nm and 625-nm absorption data. FTA and simulated emission data are also used to attribute a red-shifted absorption to I-460.[23,24] The structural characterization of these intermediates can be achieved with vibrational spectroscopy generated with pulsed laser excitation (e.g., Raman scattering), but only if vibrational data with sufficient spectral resolution can be obtained within their femto/picosecond lifetimes (neither I-460 nor J-625 have been stabilized at low temperature). Given the inverse relationship between vibrational bandwidth and laser pulse widths (based on transform-limited optical pulses), vibrational Raman data of useful bandwidths are available only for intermediates having significant populations within ~2 ps and longer of the photocycle initiation (e.g., J-625[7] and K-590[25,26] in the BR photocycle). Of particular relevance here are the retinal structural changes observed in picosecond time-resolved CARS (PTR/CARS) vibrational spectra establishing that C_{13}═C_{14} isomerization occurs as J-625 transforms into K-590.[7]

Although the BR6.9 artificial BR pigment has been shown to have a full photocycle,[18] differences between the BR6.9 and native BR photocycles are observed in the rates by which the respective photocycle intermediates undergo transformations:

formation and decay of the J6.9 and K6.9 are comparable (J6.9 → K6.9 is 5 ps and K6.9 → L6.9 is 10 ns[18]) to those of native BR-570 (J-625 → K-590 is 3.5 ps and K-590 → L-550 is ∼1 μs[27,28]). Thus, PTR/CARS data from the K-like intermediate can be readily measured, but the analogous vibrational data from the J-like intermediate are difficult to obtain given its short lifetime. Attention here is primarily given to the structural changes assignable to K6.9.

In this paper, picosecond resonance (PR/CARS) data are recorded from ground-state BR6.9 in both its light- and dark-adapted forms, while PTR/CARS data over several time delays are collected from BR6.9 photocycle intermediates. In all of these cases, the focus is on determining the vibrational degrees of freedom in the respective retinal chromophores. PR/CARS spectra from light- and dark-adapted BR6.9 and PTR/CARS spectra from K6.9 independently reveal distinct retinal structures that are not readily assignable to either all-*trans*- or 13-*cis*-like configurations. Of special interest is the elucidation of the isomeric forms of the retinals in BR6.9 and K6.9 and a determination of whether C_{13}═C_{14} isomerization occurs within the BR6.9 photocycle. Although the presence of a six-membered ring in BR6.9 does not directly prevent C_{13}═C_{14} isomerization, its presence alters both the kinetic properties underlying the formation and decay of K6.9 (*vide supra*) and the overall structures of BR6.9 and K6.9.

Experimental Section

A. Materials. BR is grown from a cell line of *Halobacterium salinarium* and is purified according to established methods.[29] The quality of the BR sample is determined by the ratio between the protein absorption at 280 nm and the retinal absorption of the light-adapted purple membrane at 570 nm (1.5 for all BR samples used in this study).

Bacterioopsin is isolated from BR by removing the all-*trans* retinal found in native BR by a bleaching process: the native BR solution containing 1 M NH_3OHCl, 1 M NaOH, and 1 M NaCl buffered at pH = 7.0 is exposed to the focused output from a 500-W projector lamp that passes through a 450-nm cutoff filter. After complete bleaching, a 10 mM K_2HPO_4/dithiothreitol (DTT) buffer and a 5% v/v solution of bovine serum albumin (BSA) is added to the BR solution to remove the hydroxylamine and any excess all-*trans* retinal. The resultant solution undergoes ultracentrifugation and is washed with deionized water three times.

The structurally modified chromophore, retinal 6.9 (all-*trans*-9,11-propanediylretinal), containing a six-membered carbon ring bridging the C_9═C_{10}−C_{11} bonds, is synthesized according to previously described methods.[18] The retinal 6.9 chromophore is dissolved in ethanol (2% of the total volume of buffered opsin solution using a 1:1 molar ratio of opsin to retinal). The reconstitution of bacterioopsin with the retinal 6.9 occurs in the dark at 0 °C over several days. The reconstituted BR6.9 sample is washed with deionized water and centrifuged with BSA to obtain a pellet that is resuspended in 10 mM K_2HPO_4/1 mM DTT buffer to yield approximately 15 mL of a 3.5 OD sample in H_2O. Light-adapted BR6.9 samples are obtained by exposure to a fluorescent lamp for 20 min prior to either PTA or CARS measurements. The dark-adapted BR6.9 sample is obtained by preserving the sample in complete darkness for more than 1 h prior to PTA or CARS measurements.

B. Instrumentation and Experimental Procedures. The instrumentation used to record PTA, PR/CARS, and PTR/CARS signals simultaneously utilizes two or three picosecond dye lasers that are synchronously pumped by the second harmonic output of a continuous wave (CW), mode-locked Nd:YAG laser. The relative timing between these picosecond laser pulses is controlled by an optical delay line system. The same optical system also provides the control of the spatial and angular orientation of the two or three picosecond laser pulses within the flowing BR sample needed to quantitatively measure CARS signals using a triple monochromator/multichannel detection system. The overall laser and spectroscopic instrumentation is described in detail elsewhere[26,30], and therefore, only a brief overview is provided here.

The 1064-nm output (80 ps pulses at 76 MHz repetition rate) of a CW mode-locked Nd:YAG laser (Coherent, Antares 76) is used to generate second harmonic radiation at 531 nm from a lithium triborate (LBO) crystal. The 531-nm radiation is used to pump three, independently controlled picosecond dye lasers (Coherent, model 701-3). Each dye laser is equipped with a cavity dumper (Coherent, models 7210 and 7220), all three of which are synchronized to the 76 MHz repetition rate of the mode locker used to operate the Nd:YAG pump laser. The output powers of the dye lasers are adjusted by controlling the 1064-nm pumping power (0.6−1 W) through a combination of polarizing beam splitters and half-lambda plates. All of the dye lasers are operated at a 400-kHz repetition rate to match the flow properties of the flowing sample[26,30] and, thereby, to exchange the sample volume measured between successive dye laser pulses.

One of the driving fields for the CARS signal, ω_1, is obtained as a narrow bandwidth (<4 cm^{-1}, fwhm), 663-nm output from a dye laser (DCM dye, 30 nJ/pulse) operating with an intracavity, three-plate birefringent filter. The autocorrelation width (fwhm) of these laser pulses, as measured by a rapidly scanned autocorrelator, is ∼7.5 ps, and the corresponding individual temporal pulse widths are ∼5.5 ps (assuming Gaussian pulse shapes).

The second driving field for the CARS signal, ω_s, is obtained as a broad bandwidth, picosecond output from a synchronously pumped CW mode-locked dye laser operating without an intracavity birefringent filter. The ∼700 cm^{-1} (fwhm) broadband output of this dye laser, using an LD740 (Exciton) dye, covers the Stokes spectral region (ω_s) needed to generate CARS signals in the 760−1750 cm^{-1} range. The experimental conditions are optimized to obtain the maximum output energy (typically 20 nJ/pulse) and the shortest pulse width (∼7.5 ps). Power measurements are made with a calibrated photovoltaic device (Coherent, model 212).

Expanding (X5) telescopes are used to control the divergence of the ω_1 and ω_s beams and, thereby, the spatial overlap of the ω_1 and ω_s beams within the flowing sample. This expansion of the laser beams also minimizes the change in beam diameter caused by the movement of the retroreflectors that comprise the optical delay lines. The spatial separation between the ω_1 and ω_s beams, and therefore the phase matching angle between the two focused beams in the sample, is controlled by varying the position of the mirror that reflects the ω_s beam onto a pellicle beam splitter. The phase-matching angle expected for the BR sample is calculated for a water sample and is adjusted to obtain the maximum CARS signal.

CARS signals are generated simultaneously from two separate sample compartments containing either a reference solution (water) or the sample protein.[30] This configuration compensates for any long-term changes in the laser intensities and spectral shapes and the resultant effect on the CARS signal. The sample compartment is comprised of the flowing BR solution formed into a jet stream through a capillary nozzle (400 μm diameter,

12 m/s). The reference compartment is a capillary containing a static water sample placed next to the nozzle. For PR/CARS data, this configuration permits the simultaneous measurement of a nonresonant CARS background signal from water[31] and a resonant CARS signal from the protein. Thus, the two CARS signals can be normalized to minimize variations in the spectral response due to spatial fluctuations in the sample. Both CARS signals are dispersed through a three-stage spectrometer (SPEX Triplemate) and onto two parallel channels of a liquid-nitrogen-cooled, two-dimensional CCD detector (EG&G 256 × 1024).

The BR6.9 photocycle is initiated via optical excitation (570 nm, <3 ps laser pulse, and 5 nJ/pulse). The excitation beam enters the sample as a counterpropagating beam relative to the direction of the ω_1 CARS probe beam, thereby minimizing any residual linear and nonlinear scattering signals that might otherwise be present. PR/CARS and PTR/CARS signals are recorded in alternating order of time delays to facilitate the direct comparison of the signals from BR6.9 and from the reactive mixtures of the BR6.9 and its photocycle intermediates.

CARS spectra are quantitatively fitted with a model function representing the third-order nonlinear susceptibility ($\chi^{(3)}$) relationships describing CARS phenomena.[30] By using a nonlinear fitting procedure, the parameters (band origin position, amplitude, bandwidth, and relative electronic phases[30]) describing each vibrational mode in a given species (stable and intermediate) can be derived.[26]

Results

A. Absorption Spectrum of BR6.9. Because the absorption spectra of native BR-570 and BR6.9 are, in general, similar (Figure 1), the replacement of the all-*trans* retinal (BR-570) with the retinal analogue all-*trans*-9,11-propanediylretinal (retinal 6.9) to form the artificial pigment BR6.9 must not significantly alter the electron delocalization throughout the entire polyene chain that forms the backbone of the protein chromophore. This similarity, however, does not exclude the possibility that electron delocalization within the polyene chain changes at specific bonds or in a particular bonding region, effects that can be monitored by vibrational spectroscopy.

To facilitate comparisons of vibrational data and to simplify the $\chi^{(3)}$ analysis, the ω_1 and ω_s values used to generate both PR/CARS and PTR/CARS signals from BR-570 and BR6.9, and their respective photocycle intermediates, are selected to be the same (Figure 1). As a consequence, any differences in the vibrational Raman spectra from BR-570 and BR6.9 cannot be attributed to changes in the degree of resonance enhancement caused by differences in the excitation wavelengths used to generate CARS signals (i.e., ω_1 and ω_s are the same). The same conclusion can be correctly reached for comparisons of CARS spectra from K-590 and K6.9 or from J-625 and J6.9.[25,26] Rather, any changes in the relative intensities of vibrational bands are attributable to alterations in the retinal structure or electron delocalization at specific locations within the retinal chromophore or both. The small differences in the respective absorption spectra (i.e., resonance enhancements) are unlikely to account for significant changes in the respective vibrational spectra.

B. PR/CARS Spectrum of BR6.9. The vibrational spectra (800−1700 cm^{-1}) of BR-570 and BR6.9 are significantly different, a result that can be attributed to the differences in retinal bonding and structure associated with the introduction of the six-membered ring bridging the C_9═C_{10}−C_{11} positions.[14] PR/CARS data are recorded from the light-adapted BR6.9 over two spectrally overlapping regions, each ∼500 cm^{-1} wide

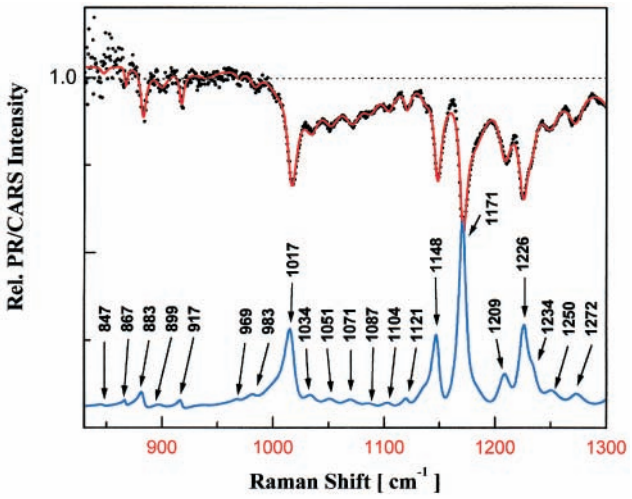

Figure 2. PR/CARS spectrum of BR6.9 in the 830−1300 cm^{-1} region. The nonresonant CARS signal from water only, indicated by the horizontal dashed line, is used to normalize the PR/CARS signal. The $\chi^{(3)}$-fit function is shown as a solid line overlapping the PR/CARS data (●). The corresponding background-free (Lorentzian line shape) vibrational CARS spectrum of BR6.9, derived from the $\chi^{(3)}$-fit, is shown at the bottom. The wavenumber positions of selected bands are presented. The $\chi^{(3)}$-fit parameters and a complete list of band origins found are presented in Table 1.

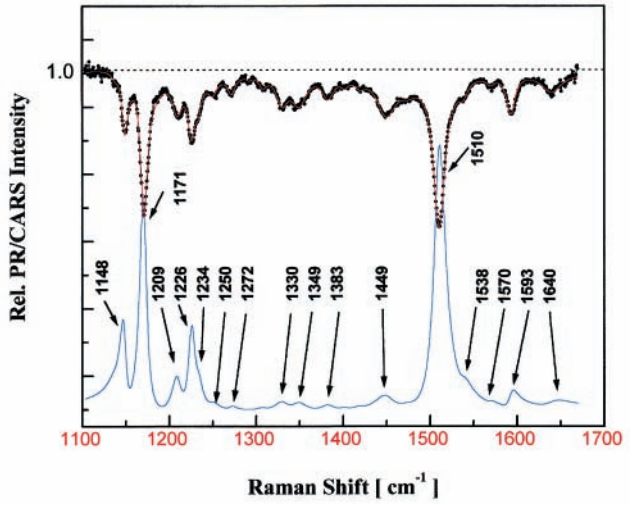

Figure 3. PR/CARS spectrum of BR6.9 in the 1100−1650 cm^{-1} region. The nonresonant CARS signal from water only, indicated by the horizontal dashed line, is used to normalize the PR/CARS signal. The $\chi^{(3)}$-fit function is shown as a solid line overlapping the PR/CARS data (●). The corresponding background-free (Lorentzian line shape) vibrational CARS spectrum of BR6.9, derived from the $\chi^{(3)}$-fit, is shown at the bottom. The wavenumber positions of selected bands are presented. The $\chi^{(3)}$-fit parameters and a complete list of band origins found are presented in Table 1.

(Figures 2 and 3). The 663-nm wavelength of ω_1 is selected to appear on the low-energy side of the BR6.9 absorption spectrum (Figure 1) to minimize any contributions to the CARS signal from photocycle intermediates that may be produced by the ω_1 probe (5 ps) pulse.

The $\chi^{(3)}$-fitting function provides background-free Lorentzian line shape CARS spectra assignable to BR6.9 (Figures 2 and 3). The $\chi^{(3)}$-fitting parameters (band origins, Ω_i, bandwidth, Γ_i, and amplitudes, A_i) utilized for the PR/CARS data from BR6.9 are presented in Table 1. The error in measuring the band origin position of a given vibrational feature is ∼1 cm^{-1}. A comparison of the data from BR-570 and BR6.9 shows that both the PR/

TABLE 1: Band Positions (Band Maxima for Resonance Raman (RR) and Origins, Ω_k for (PR/CARS)) in Vibrational Spectra Recorded from BR6.9, BR-570, and BR5.12 with Vibrational Mode Assignments Presented for Selected Features

BR6.9		vibrational modes assignment[c,d]	BR-570	BR5.12
RR[a] max (cm^{-1})	PR/CARS[b] Ω_k (cm^{-1})		PR/CARS[e] Ω_k (cm^{-1})	PR/CARS[f] Ω_k (cm^{-1})
			830	
850	847		850	
	867			
	883	C_{10}−, C_{11}−, C_{14}−H wag	883	890
	899			
	917			
	938			
	969	C_7−C_8 HOOP	959	971
	983	C_{15}−H wag	982	1001
1012	1017	CH_3(19/20) rocking	1008	1020
	1034	β-ionone ring		
	1051	CH_3(19/20) rocking	1048	1050
	1071			1071
	1087			1094
	1104			
	1121		1122	1122
				1139
1143	1148	six-membered ring		
1165	1171	C_{10}−C_{11} stretching	1171	
			1185	1182
1204	1209	C_{14}−C_{15}	1202	1205
1222	1226	C_8−C_9		1229
	1234	C_{12}−C_{13} stretching		
	1250	C_{11}−H wag	1254	1259
	1272		1274	1279
	1307			1310
1331	1330	NH in-plane	1324	1331
	1349	CH_3 (19/20)	1349	
	1383	symmetric deform	1395	1380
1447			1435	1430
	1449		1456	1457
	1474			
1507	1510	C_{11}=C_{12}, C_{13}=C_{14}	1526	1516
	1538		1580	
				1551
	1570	C_{13}=C_{14}, C_9=C_{10}		1567
1589	1593	C_7=C_8, C_5=C_6	1601	1597
1629	1640	Schiff base	1638	1631

[a] Delaney, J. K.; Atkinson, G. H.; Sheves, M.; Ottolenghi, M. *J. Phys. Chem.* **1995**, *98*, 7801−7805. [b] This work, Figures 2 and 3. [c] Mathies, R.; Lin, S.; Ames, J.; Pollard, W. *Annu. Rev. Biophys. Chem.* **1991**, *20*, 491−518. [d] Brack, T. L.; Atkinson, G. H. *J. Mol. Struct.* **1989**, *214*, 289−303. [e] This work (excitation conditions are the same as those used for PR/CARS from BR6.9). Atkinson, G. H.; Ujj, L.; Zhou, Y *J. Phys. Chem. A* **2000**, *104*, 4130−4139. [f] Ujj, L.; Zhou, Y.; Sheves, M.; Ottolenghi, M.; Ruhman, S.; Atkinson, G. H. *J. Am. Chem. Soc.* **2000**, *122*, 96−106.

CARS signals themselves and the respective background-free Lorentzian line shape CARS spectra are distinct, *vide infra*.

C. Vibrational Mode Assignments for BR6.9. Of the 33 vibrational bands found in the PR/CARS spectrum of BR6.9 (Figures 2 and 3), only 11 vibrational bands had been observed in the corresponding resonance Raman (RR) spectrum of BR6.9.[18] The BR6.9 bands are anticipated to be assignable to modes that are analogous to those found in BR-570, except to the degree that the six-membered ring found in BR6.9 perturbs vibrational degrees of freedom in retinal. Comparisons with the vibrational spectra (PR/CARS and RR) from other artificial BR pigments containing ring structures (BR5.12[17] and BR6.11[32]) are also used to facilitate vibrational mode assignments.

1. Hydrogen Out-of-Plane (HOOP) and C−CH_3 Rocking Modes. The vibrational bands at 847, 867, 883, 899, 917, and 938 cm^{-1} can be associated with hydrogen wagging and HOOP modes in BR6.9. By analogy with the vibrational mode assignments in BR-570 (883 cm^{-1} [7−9]), BR6.11 (880 cm^{-1} [32]), and BR5.12 (890 cm^{-1} [17]), the most intense BR6.9 band at 883 cm^{-1} can be assigned to the hydrogen wagging motions at C_{10}, C_{12}, and C_{14}. Because the six-membered carbon ring and the β-ionone ring are relatively close spatially with the BR6.9 retinal, the distribution of electron density within the polyene chain between C_7 and C_{12} is anticipated to generate a relatively repulsive force. As a consequence, degenerate out-of-plane modes involving hydrogen motion (e.g., those near C_{10} and C_{12}) are expected to appear more prominently in Raman spectra. The increased Raman activity of the 883-cm^{-1} band is consistent with such an analysis. The relatively isolated bands at 969 and 983 cm^{-1}, with counterparts at 959 and 982 cm^{-1} in BR-570,[8,9] can be assigned, respectively, to the HC_7−C_8H HOOP and C_{15}−H wagging modes.

The intense band at 1008 cm^{-1} in BR-570 can be assigned primarily to symmetric, in-plane rocking modes involving the methyl groups located at C_{19} and C_{20} (C−CH_3 rocking vibrations).[8] The absence of a band near around 1008 cm^{-1} in the PR/CARS spectrum of BR6.9 can be attributed to the absence of a CH_3 group at C_{19} (Figure 1), while the appearance of a relatively intense band at 1018 cm^{-1} can be attributed to the single methyl-rocking mode originating with the C_{20}−CH_3 motion. These assignments are consistent with those made for the analogous bands in BR5.12 (at 1020 cm^{-1} for the CH_3 rocking modes at C_{19} and C_{20}[17]) and in BR6.11 (at 1017 cm^{-1} for the CH_3 rocking mode at C_{19}[32]).

The relatively weak 1048-cm^{-1} band in BR-570, assignable to an out-of-plane C_{20}−CH_3 rocking mode,[8,9] can be associated

with the same mode in BR6.9, having a band appear at 1051 cm^{-1}. Analogous bands are observed in both BR5.12[17] and BR6.11.[32]

The BR6.9 vibrational bands at 1034, 1087, 1109, and 1121 cm^{-1} have counterparts in the BR-570 spectrum that are assigned to modes in the β-ionone ring.[8,18] Although similar assignments for the BR6.9 bands are appropriate, the evident changes in positions and relative intensities observed in BR6.9 are likely attributable to the electronic interactions between the six-membered carbon ring and the β-ionone ring present in BR6.9. Similar vibrational band structure is observed in the 1030−1130-cm^{-1} region of the BR6.11 PR/CARS spectrum[32] but with fewer bands, an observation that may be associated with the greater distance between the six-membered carbon ring and the β-ionone ring (i.e., reduced electronic interaction), *vide infra*.

The bands near 1445 cm^{-1} can be associated with the deformation of the CH_3 group through the assignments of analogous bands in the vibrational spectra of both BR-570[8,9] and BR5.12 (the 1430-cm^{-1} band is assigned to the $C_{20}-CH_3$ rocking mode[17]).

2. C−C Stretching Modes. The pattern of vibrational bands in the C−C stretching (fingerprint) region is significantly different in the native BR-570 than in its artificial pigments: BR5.12,[17] BR6.11,[32] and BR6.9 (Figure 2). The fingerprint bands are assigned to the C−C stretching modes that are strongly coupled to C−C−H rocking modes.[8−10] These C−C stretching bands have been repeatedly used to identify the isomeric structure of retinal as either all-*trans* or 13-*cis*.[10,26,33] Four intense bands at 1148, 1171, 1209, and 1226 cm^{-1} are observed in BR6.9, only three of which have clearly identifiable counterparts in the vibrational spectrum of BR-570. Among these four bands, the 1148-cm^{-1} band appears only in the BR6.9 spectrum.

The intense 1148-cm^{-1} band can be associated with the six-membered carbon ring in BR6.9 because an analogous 1142-cm^{-1} band is observed as an intense feature in the vibrational spectra of compounds such as cyclohexene and its derivatives.[34] None of the other vibrational bands of significant intensity found in the spectra of cyclohexene-type compounds (e.g., at 1171 and 1209 cm^{-1}), however, are observed in the spectrum of BR6.9. In addition, no similar band is observed near 1148-cm^{-1} in BR6.11, although it contains the same six-membered carbon ring incorporated at the $C_{11}=C_{12}-C_{13}$ positions.[32] The assignment of the 1148-cm^{-1} band to modes in the six-membered carbon ring, therefore, must be based on a factor(s) specific to the electronic properties of BR6.9 that would increase its Raman intensity relative to all other cyclohexene-type modes.

Such an enhanced Raman activity may be attributable to one or more of the structural differences between BR6.9 and BR6.11. The most evident differences are derived from the changes in distance between the carbon rings and the β-ionone ring. Because it can be anticipated that some degree of resonance interaction involving delocalized electron energy within the polyene chain exists between the two rings, their proximity to each other should significantly influence the relative magnitude of electron delocalization. In addition, each carbon ring has both a direct and a secondary effect on the interaction(s) between specific regions of the retinal (altered in general by the introduction of a carbon ring) and specific parts of the protein binding pocket. An example of the former is the removal of the $C_{19}-CH_3$ group in BR6.9, which alters the interaction between tryptophan 182 and the $C_{19}-CH_3$ in-plane rocking mode. An example of the latter is the effect that the carbon ring in BR6.9 has on the retinal structure in the Schiff-base region. Because the electrostatic interaction(s) between the protonated C=N bond in the Schiff-base region and its adjacent amino acids is greatly influenced by their distance of separation, the rigidity or spatial changes or both in the retinal associated with the incorporation of the carbon ring may alter the Schiff-base protonation mechanism, a major component in the overall BR photocycle. Either one or both of these factors may underlie the increased 1148-cm^{-1} band intensity in the BR6.9 PR/CARS spectrum.

Increased Raman intensity can be assigned to the out-of-plane twisting/distortion of the polyene chain. For example, an analogous band at 1144 cm^{-1} is observed in the PTR/CARS spectrum of the T5.12 intermediate formed in the BR5.12 photoreaction.[17] Independent vibrational band assignments show T5.12 to have a twisted/distorted polyene structure.[17] The same twisted/distorted polyene description can be applied to BR6.9, a conclusion supported by the increased HOOP mode intensities observed in its PR/CARS spectrum (Figure 2). The presence of a six-membered ring in the polyene chain, especially having significant electronic resonances with the adjacent β-ionone ring, can be anticipated to result in a twisted/distorted polyene chain, thereby enhancing the intensity of the 1148-cm^{-1} band in ground-state BR6.9. On the basis of these points, the 1148-cm^{-1} band can be assigned to the C_6-C_7 stretching mode.

Vibrational spectra from BR-570 and from artificial BR pigments in which no similarly intense bands near 1148 cm^{-1} appear support this assignment. The bands assigned to the C_7-C_8 stretching mode in BR-570 at 1135 cm^{-1},[7−9] in BR6.11 at 1137 cm^{-1},[32] and in BR5.12 at 1139 cm^{-1},[17] are not altered by the incorporation of a carbon ring. In BR6.11 and BR5.12, however, the distances between the respective carbon rings and the β-ionone ring are larger than in BR6.9. In BR-570, of course, there is no additional ring with which the β-ionone ring can resonantly interact. Only in BR6.9 in which the separation between the carbon ring and the β-ionone ring is small does the position and intensity of the C_6-C_7 band (1448-cm^{-1} band) change.

The mode assignments of the 1171-cm^{-1} band in BR6.9 can be derived directly from those in BR-570 in which an 1171-cm^{-1} band also appears and is assigned to have $C_{10}-C_{11}$ stretching character with some coupling to the $C_{11}-C_{10}-H$ rocking motion.[9] The bands at 1209 and 1226 cm^{-1} in BR6.9 can similarly be assigned to $C_{14}-C_{15}$ or C_8-C_9 stretching modes, although their BR-570 counterparts appear, respectively, at 1202 and 1212 cm^{-1}.[8] The respective ∼7 and ∼14 cm^{-1} increase in these band frequency positions for BR6.9 can be attributed to the C_8-C_9 stretching mode (affected directly by the incorporation of the carbon ring, Figure 1). The positions of the analogous bands in BR5.12 (1205 and 1229 cm^{-1}) also increase when the five-membered ring spanning $C_{12}-C_{13}=C_{14}$ is incorporated (thereby changing the coupling contributions of the $C_{13}=C_{14}$ mode).

3. C=C Stretching and Schiff-Base Modes. The PR/CARS spectrum of BR6.9 contains four bands in the C=C stretching region (1510, 1538, 1570, and 1593 cm^{-1}, Figure 3) and one band in the Schiff-base region (1640 cm^{-1}, Figure 3). These vibrational band patterns are substantially different than those in the BR-570 spectrum.[31] The position of the most intense BR-570 band at 1527 cm^{-1}, assigned to the $C_7=C_8$, $C_{11}=C_{12}$, and $C_{13}=C_{14}$ stretching modes, shifts to 1510 cm^{-1} in BR6.9, while the relative intensities of the other C=C stretching bands decrease significantly in BR6.9. Because similar phenomena are also observed in both BR6.11 (1510 cm^{-1})[32] and BR5.12

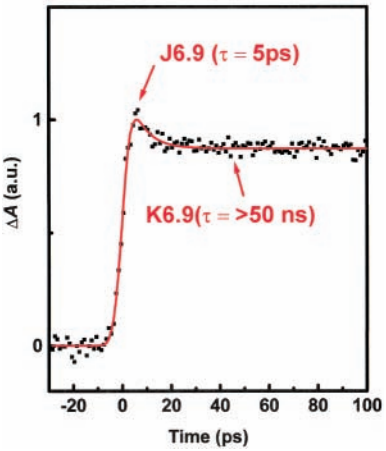

Figure 4. PTA data (■ points) for BR6.9 obtained following 570-nm excitation and for a 663-nm probe wavelength over the −30 to 100 ps (3-ps time resolution) time period. The kinetic trace (solid line) is obtained from a global fit of the PTA data. The PTA features used to identify J6.9 (5 ps decay constant) and K6.9 (>50 ns lifetime) are shown.

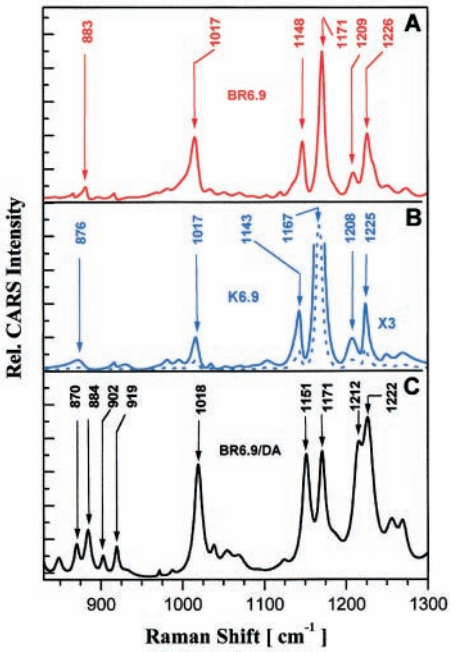

Figure 5. Background-free (Lorentzian line shape) vibrational CARS spectra of (A) BR6.9 (recorded via PR/CARS), (B) K6.9 (recorded via PTR/CARS with a 50-ps time delay and including a ×3 expanded intensity scale), and (C) dark-adapted BR6.9 (recorded via PR/CARS) in the 830−1300 cm^{-1} region. The CARS spectra of K6.9 are the same from PTR/CARS data recorded at 50, 100, and 200 ps time delays. The wavenumber positions of selected bands are presented.

(1516 cm^{-1}),[17] its source appears to be associated with the general incorporation of a carbon ring somewhere in the polyene chain. The independence of both the band position shifts and the decreased intensities on the precise location of the carbon ring in the polyene chain suggests that, in each case, the delocalized electron density along the polyene chain is altered. These correspond to an alteration in the retinal geometry (e.g., the degree of retinal planarity within the binding pocket). Thus, the 1510-cm^{-1} band in BR6.9, in analogy with the bands appearing the vibrational spectra from BR6.11[32] and BR5.12,[17] can be assigned to the C_7═C_8, C_{11}═C_{12}, and C_{13}═C_{14} stretching modes.

The less intense bands appearing as shoulders at 1580 and 1601 cm^{-1} in BR-570 and assigned mainly to the C_9═C_{10} and C_{13}═C_{14} antisymmetric vibrations with small contributions from the C_5═C_6 stretching mode[8−10,33] are observed as three separate bands in BR6.9 at 1538, 1570, and 1593 cm^{-1}. The band at 1640 cm^{-1} in BR6.9 can be assigned to the C═N stretching mode associated with the protonation state of the Schiff-base and its lysine linkage to the opsin.[8−10,17,33] Unlike the decrease of the Schiff-base band to 1631 cm^{-1} in BR5.12[17], which is attributed to interactions with its five-membered, carbon ring, or an altered Schiff-base environment induced by the five-membered ring, the frequency of the Schiff-base band in BR6.9 is the same (within the <2 cm^{-1} experimental error for a weak feature) as that in native BR-570 (1638 cm^{-1}).

The assignment of the weak 1349-cm^{-1} band in BR6.9, as for the 1348 cm^{-1} band in BR-570, involves the NH in-plane rocking mode. The relatively small position change from the BR-570 band indicates that the carbon ring in BR6.9 has little effect on the NH part of the polyene chain, which is in contrast to the large decrease in the position of this mode (1331 cm^{-1}) observed in BR5.12 in which the carbon ring (five-membered) directly alters the NH motion.[17]

D. PTA Data for the BR6.9 Photocycle. PTA data (ΔA) are measured (probe wavelength of 663 nm) over the initial 200 ps of the BR6.9 room-temperature photocycle following 3-ps, 570-nm excitation of BR6.9 (Figure 4). These PTA data clearly identify the presence of two intermediates, J6.9 and K6.9, both of which have been previously reported.[18] The improved quality of these PTA data (Figure 4), however, permits a more accurate determination of the rate constants (τ) describing the kinetics underlying the formation and decay of J6.9 and K6.9 than that available from earlier data:[18] J6.9 → K6.9 occurs with a $\tau = 5 \pm 1$ ps, while the K6.9 concentration remains constant over the 15 ps to 54 ns time interval measured. PTA data are recorded during each PTR/CARS experiment to independently measure the relative concentrations of BR6.9, J6.9, and K6.9 (used in the quantitative $\chi^{(3)}$ analysis of the CARS data) and to accurately determine the 0-ps time point.

E. PTR/CARS Spectrum of K6.9. PTR/CARS spectra are recorded at six delay intervals (0, 5, 10, 50, 100, and 200 ps) throughout the initial 200 ps of the BR6.9 photocycle using the simultaneously recorded PTA signals to quantitatively determine the absolute time scale as well as the delay intervals. Attention is focused on the vibrational spectrum of K6.9, which has a relatively long lifetime (∼5 ps to >54 ns). The resultant background-free CARS spectrum of K6.9 (800−1700 cm^{-1}), derived from the PTR/CARS spectrum recorded at 50 ps, is presented in two spectrally overlapped regions each ∼500 cm^{-1} wide (bottom of Figures 5 and 6). The same background-free CARS spectrum of K6.9 is obtained from three independent PTR/CARS measurements at 50, 100, and 200 ps, all delay times at which the concentration of K6.9 has been shown from PTA data to be constant. To facilitate comparisons, the background-free CARS spectrum of BR6.9 is presented at the top of Figures 5 and 6.

F. Vibrational Mode Assignments for K6.9. The appearance of the same vibrational bands, distinct from those in the PR/CARS spectrum of BR6.9 (Figures 5 and 6), in the background-free CARS spectra obtained from PTR/CARS data recorded at 50, 100, and 200 ps spectra demonstrates that K6.9 can be described as an intermediate with well-defined vibrational modes over this time interval and a molecular structure that is distinct from that of BR6.9.

1. HOOP and CH_3-Rocking Modes. The CARS bands for K6.9 appearing at 876, 917, and 933 cm^{-1} can be assigned to

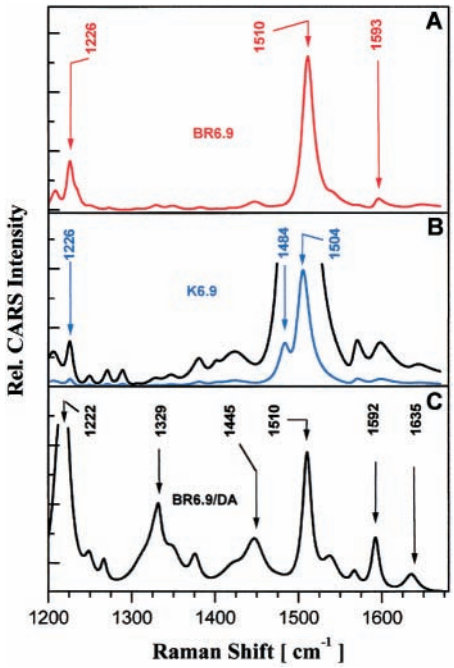

Figure 6. Background-free (Lorentzian line shape) vibrational CARS spectra of (A) BR6.9 (recorded via PR/CARS), (B) K6.9 (recorded via PTR/CARS with a 50-ps time delay and including a ×3 expanded intensity scale), and (C) dark-adapted BR6.9 (recorded via PR/CARS) in the 1100−1650 cm^{-1} region. The CARS spectra of K6.9 are the same from PTR/CARS data recorded at 50, 100, and 200 ps time delays. The wavenumber positions of selected bands are presented.

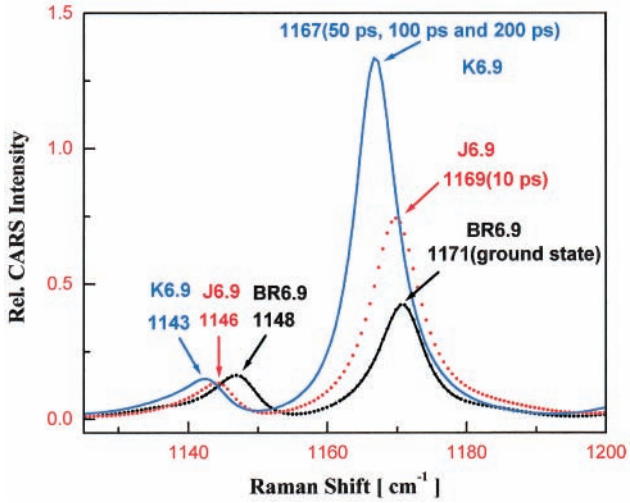

Figure 7. Time evolution of the C−C stretching (fingerprint) CARS bands assigned to BR6.9, J6.9, and K6.9. PR/CARS data from BR6.9 and PTR/CARS data recorded for 10, 50, 100, and 200 ps time delays are shown (50, 100, and 200 ps data are the same). Focus is given to the time-dependent changes in the 1148 and 1171 cm^{-1} bands of BR6.9. Relative intensities are normalized to the intensity of the 1226-cm^{-1} band, which does not change significantly in the measured PTR/CARS (i.e., without $\chi^{(3)}$-fitting) data (see text).

hydrogen wagging and HOOP modes. Although the relative intensity of the K6.9 band at 876 cm^{-1} band is approximately the same as that of the analogously assigned 883- and 867-cm^{-1} bands in BR6.9, their respective bandwidths are substantially different (Figure 5): ∼13 cm^{-1} for K6.9 (876 cm^{-1} band) versus ∼5 cm^{-1} for BR6.9 (883 and 867 cm^{-1} bands). Such a large bandwidth difference (factor of 2.5) shows that the polyene chain in K6.9 is significantly more twisted/distorted than its ground-state BR6.9. There is no evident change in the C_{20}−CH_3 rocking modes found in BR6.9 and K6.9 (both assignable bands appear at 1017 and 1048 cm^{-1}).

2. C−C Stretching Modes. The general pattern of vibrational bands in the C−C stretching (fingerprint) region of K6.9 is similar to that of BR6.9 (Figure 5), although the relative intensities among the three major C−C stretching bands are different. The position decrease of the 1171-cm^{-1} band in BR6.9 (assigned to C_{10}−C_{11} stretching mode) to 1167 cm^{-1} in K6.9 is accompanied by a large increase in its relative intensity (normalized to the 1226-cm^{-1} band). Both the decreasing position and increasing relative intensity of the 1171 cm^{-1} band in BR6.9 are time-dependent over the interval during which K6.9 is formed (based on PTA data, Figure 4). Once the band position reaches 1167 cm^{-1} at a 50-ps delay, however, it remains unchanged throughout the 50−200-ps interval measured here, thereby indicating that the 1167 cm^{-1} band is assignable to K6.9. Taken together, these C−C stretching bands show that, even though a six-membered ring is present, the retinal in K6.9 has a modest degree of out-of-plane twisting/distortion. This conclusion is independent of whether K6.9 is generally all-*trans* or 13-*cis*.

Neither the positions nor the intensities of the other two major C−C stretching bands at 1209 and 1226 cm^{-1} (assigned, respectively, to the C_{14}−C_{15} and C_8−C_9 stretching modes) change during the initial 200-ps of the BR6.9 photocycle. The fourth band in this region, at 1148 cm^{-1}, is associated with the six-membered carbon ring in BR6.9 and decreases in position to 1143 cm^{-1} in K6.9.

3. C═C Stretching and Schiff-Base Modes. The vibrational band patterns in the C═C stretching and Schiff-base regions are substantially different for BR6.9 and K6.9. The position of the most intense BR6.9 band at 1510 cm^{-1}, assigned to C_7═C_8, C_{11}═C_{12}, and C_{13}═C_{14} stretching modes, decreases and splits to two major bands appearing at 1484 and 1504 cm^{-1} (Figure 6). Although the lower intensity bands at 1570 and 1593 cm^{-1} in BR6.9 have essentially the same positions in K6.9 (1570 and 1593 cm^{-1}), the intensity of the 1570 cm^{-1} band relative to that of the 1593 cm^{-1} band is much larger.

The very weak Schiff-base band in K6.9 appears at the same position (1639 cm^{-1}) as in BR6.9. The presence of a Schiff-base band in a K-like intermediate is new because no analogous band is observed in vibrational spectra of either the native K-590 or the artificial K-like intermediates.[25,26]

G. PTR/CARS Spectrum of J6.9. Even though the absorption spectra of all three species comprising the transient mixture, BR6.9, J6.9, and K6.9, overlap extensively throughout the visible region, the presence of J6.9 in the BR6.9 photocycle, as well as its ∼5-ps lifetime, is evident from the PTA data (Figure 4). The vibrational spectrum of J6.9, however, is difficult to record because it cannot be spectroscopically or temporally separated from either BR6.9 or K6.9. Indeed, the maximum transient J6.9 population occurs during the CCT (∼7.5 ps) of the PTR/CARS experiments described here. Because the J6.9 population for time delays of 5−10 ps is <10%, these PTR/CARS data contain mainly contributions from BR6.9 and K6.9.

Nonetheless, some characterization of the J6.9 vibrational spectrum can be derived from a comparison of PTR/CARS data recorded at time delays <10 ps with those recorded in the 50−200 ps interval and with the PR/CARS spectrum of BR6.9 (Figure 7). It is important to note that the vibrational spectrum of K6.9 remains essentially constant throughout the 50−200-ps interval (*vide supra*), and therefore, differences appearing at <10-ps can be attributed to the presence of J6.9 in the transient mixtures at these short time delays. For example, in the C−C

stretching region used to characterize retinal isomerization, distinct bands at 1146 and 1169 cm^{-1} appear in the 10-ps PTR/CARS spectrum that are not assignable to either BR6.9 or K6.9 (Figure 7). On the basis of the relative populations in the 10-ps sample mixture and the CCT of ~7.5 ps, these features can be tentatively assigned to J6.9. These initial vibrational data suggest that J6.9 has a retinal structure that lies intermediate between those of BR6.9 and K6.9 and, therefore, does not emulate native J-625 and K-590, which contain distinct all-*trans* and 13-*cis* retinals.[4−7]

H. PR/CARS Spectrum of Dark-Adapted BR6.9. As with native BR-570,[4−6] artificial BR pigments such as BR6.9 exhibit thermally reversible dark/light adaptation, which has been associated with C_{13}═C_{14} isomerization[35] (the dark-adapted form, BR-548, is assigned to have a 13-*cis* retinal[4−6]). It is useful, therefore, to examine the vibrational spectrum of dark-adapted BR6.9 (BR6.9/DA) as a potential example of the spectral features that identify a 13-*cis*-like retinal in this artificial BR pigment.

The PR/CARS spectrum (880−1700 cm^{-1}) of BR6.9/DA (Figures 5C and 6C) contains 33 assignable features and, in general, resembles the corresponding CARS spectra of BR6.9 and K6.9 (Figures 5 and 6). Careful inspection, however, reveals many vibrational features that show the configurations of each retinal in light- and dark-adapted BR6.9 and K6.9 to be distinct:

(1) The constancy of the 1017/8-cm^{-1} feature (C_{20}−CH_3 rocking mode) and the similar positions and relative intensities of the HOOP feature show that the out-of-plane structures of all three species are similar (Figure 5).

(2) Of particular importance with respect to the isomeric form of retinal are the features in the 1100−1300 cm^{-1} region. As discussed elsewhere (*vide supra*), the C−C stretching bands of BR6.9 and K6.9 are only slightly different from each other, while those of BR6.9/DA are significantly different in both positions and relatively intensities. While the 1151 and 1171 cm^{-1} features are shifted slightly, their relative intensities are dramatically different than the corresponding BR6.9 and K6.9 bands: the intensity of the 1171-cm^{-1} feature is 3−8 times larger than the respective 1151-cm^{-1} bands in BR6.9 and K6.9, while the 1171- and 1151-cm^{-1} bands are of about equal intensity in BR6.9/DA. The 1212- and 1222-cm^{-1} features in BR6.9/DA have both distinct positions and relative intensities.

Discussion

The CARS data from BR6.9 and K6.9 are used to address both the specific structural changes in the retinal during the initial 200-ps of the BR6.9 photocycle and the general molecular mechanisms describing both other artificial BR pigments and the native BR photocycle.

A. Structure of BR6.9. CARS data (Figures 2 and 3) show that, in general, the modifications to the retinal structure in BR-570 caused by the incorporation of a six-membered carbon ring spanning the C_9═C_{10}−C_{11} bonds to form BR6.9 are relatively small. Of particular importance here, the all-*trans* configuration of the retinal analogue, 9,11-propanediylretinal (retinal 6.9), used to form BR6.9 is not altered significantly once it is introduced into the bacterioopsin (i.e., BR6.9 has an all-*trans*-like retinal, as does BR-570).[7−10,33]

When these CARS spectra are examined in detail, however, significant structural differences between retinal chromophores in BR6.9 and BR-570 do appear:

(1) The primary difference in the BR-570 and BR6.9 vibrational spectra is the enhanced Raman activity (intensity) in the 1148-cm^{-1} band (Figure 2), a feature assignable to stretching modes in the carbon ring. No analogous band is observed in the spectra from BR-570,[8,9] BR5.12,[17] or BR6.11.[32] Vibrational spectra from molecules such as cyclohexene and cyclohexane, however, do contain analogous bands near 1148 cm^{-1} assigned to a ring stretching mode.[34] The increased Raman activity for such a carbon ring mode in the BR6.9 spectrum can be attributed to a specific delocalized electron interaction among the C−C and C═C bonds within the carbon and β-ionone rings and the interconnecting C_7═C_8−C_9═C_{10} bonding in the polyene chain (Figure 1). The enhanced Raman intensity derives from the proximity of the carbon ring (containing a C_9═C_{10} bond) to the 2-ionone ring which delocalizes electron energy over the entire C_5═C_6−C_7═C_8−C_9═C_{10}−C_{11} region (Figure 1). As a consequence, this part of the polyene chain assumes a different geometry (symmetry) in BR6.9 than in BR-570 or in some of the other artificial BR pigments containing a carbon ring (e.g., BR5.12 and BR6.11). The uniqueness of these delocalized interactions relative to BR6.11 and BR5.12 derives from the proximity of the carbon and 2-ionone rings and not from the presence alone of the carbon ring itself. Electron delocalization over these bonds cannot occur in BR-570, BR5.12, or BR6.11 because the carbon ring either is not present or is spatially well-removed from the 2-ionone ring, thus the absence of vibrational bands analogous to the 1148-cm^{-1} band in BR6.9. Such a perturbation alters the normal vibrational modes as well as their respective Raman scattering cross sections and accounts for the intensity of the 1148-cm^{-1} band.

(2) The number and intensities of HOOP modes appearing in the BR6.9 spectrum are significantly larger than those found for BR-570,[8−10,33] BR5.12,[17] or BR6.11.[32] These features indicate that, regardless of the six-membered carbon ring, the polyene chain in BR6.9 contains significant out-of-plane motion consistent with a twisted/distorted retinal backbone. This altered retinal geometry may also be associated to some extent with the extended electron delocalization involving the carbon and 2-ionone rings, vide supra.

(3) Because the six-membered carbon ring in BR6.9 eliminates the C_{19} methyl group (Figure 1), the band assigned primarily to the symmetric, in-plane rocking modes involving both C_{19}−CH_3 and C_{20}−CH_3 in BR-570 (1008 cm^{-1})[8] is absent. Rather, a single band of enhanced intensity appears in BR6.9 at 1017 cm^{-1}. This feature can be assigned to the only in-plane CH_3-rocking mode remaining, namely, that involving the C_{20}−CH_3 bond.

(4) The general pattern of major bands (with the exception of the 1148-cm^{-1} band) observed in the BR6.9 fingerprint region (at 1171, 1209, and 1226 cm^{-1}, Figures 2 and 3) is similar to that found in the BR-570 spectrum,[31] thereby demonstrating that the retinal configuration in BR6.9 is all-trans-like (cf. BR-570[9,26]). The differences observed in relative intensities and absolute positions of the respective fingerprint bands can be attributed to changes in the overall retinal geometry, a factor independently reflected in the larger degree of out-of-plane (HOOP) motion in the ground state and the appearance of the 1148-cm^{-1} band, vide supra.

(5) The band maximum position of the strong C═C band (1510 cm^{-1}) is significantly lower (~16 cm^{-1}) in BR6.9 than in BR-570.[9,26] Analogous C═C stretching frequencies have been associated with the incorporation of a carbon ring (smaller C═C stretching frequencies appear in BR5.12[17] and BR6.11[32]). Such a reduced C═C stretching frequency indicates that the delocalized electronic energy within the polyene chain is

traceable to the carbon ring itself, regardless of where it is placed between C_9 and C_{14} within the polyene chain.

B. Structure of K6.9. Their respective vibrational spectra show that the retinal structures in BR6.9 and K6.9 are distinct, except with respect to their general isomeric configurations (Figures 5 and 6). While PTR/CARS spectra demonstrate that several types of vibrational modes change continuously as K6.9 is formed during the 10−200-ps interval of the BR6.9 photocycle, no significant changes in the C−C stretching bands occur (Figure 5).

As with other BR photocycle intermediates,[7−10] the positions and intensities of the C−C stretching (fingerprint) bands in the 1140−1250 cm^{-1} region are used to characterize the isomeric structure of retinal in K6.9. The C−C stretching band pattern observed for K6.9 closely resembles that observed for BR6.9 (Figure 5), with the notable difference being the 4−5-cm^{-1} decrease in the maxima positions for all four bands as K6.9 forms. Independently, neither the general band intensity pattern nor the absolute positions of the C−C stretching bands for K6.9 correlate directly with those found for native K-590[11,12] in which the strong, broad feature near 1196 cm^{-1} that replaces the 1171- and 1202-cm^{-1} bands in BR-570 is used to identify a 13-*cis* retinal.[9,26]

The significant changes in the relative intensities of the C−C stretching bands are evident when these band intensities are normalized. Because the 1226-cm^{-1} band intensity in PTR/CARS data (without $\chi^{(3)}$-fitting, Figures 2 and 3) remains essentially constant over the 10−200-ps period, this band can be used to normalize the remainder of the PTR/CARS band intensities. On the basis of this procedure, the relative intensity of the 1171-cm^{-1} band (BR6.9) is found to decrease by a factor of >3 over the initial 50-ps time interval of the BR6.9 photocycle (Figure 7). The intensity of the 1167-cm^{-1} band (K6.9), formed by the corresponding band maximum 4-cm^{-1} shift, remains unchanged over the subsequent 50−200 ps interval (Figure 7). A separate 20% decrease of the 1146-cm^{-1} band intensity (BR6.9) together with a 5-cm^{-1} band position decrease to 1143 cm^{-1} also can be observed in these data as K6.9 forms within the initial 50 ps (Figure 7). The positions and intensity of the 1143-cm^{-1} band then remain unchanged over the subsequent 50−200-ps interval.

Specific differences in the BR6.9 and K6.9 retinal structures involve (i) changes in electron delocalization along the polyene chain (C═C stretching modes), (ii) altered out-of-plane motion (HOOP modes), and (iii) increased interactions between retinal and its protein environment (in-plane CH_3 rocking modes):

(1) Based on the same normalization procedure used for C−C stretching modes (1226-cm^{-1} band), the relative intensity of the C═C stretching band at 1510-cm^{-1} band (BR6.9) increases by >5 as K6.9 is formed within 50 ps and then remains constant over the 50−200 ps interval. The corresponding position shift of 6 cm^{-1} follows the same time dependence. In addition, the 1484-cm^{-1} band, assignable only to K6.9, exhibits the same time dependence as that found for the 1510-cm^{-1} feature. These changes in band positions and intensities reflect, at least in part, differences between the respective degrees of electron delocalization within the polyene chains of BR6.9 and K6.9. The appearance of a new band at 1484 cm^{-1} for K6.9 suggests that these changes in electron delocalization result in isolating, and thereby energetically separating, the C═C stretching modes. Such separation is not associated with the introduction of the six-membered carbon ring (a 1484-cm^{-1} band is not in the BR6.9 spectrum), but is directly related to the photocycle process(es) underlying K6.9 formation. The appearance of the 1484 cm^{-1} band, of course, may also be associated with structural changes in the retinal that precede a redistribution of electron energy along the polyene chain.

(2) The differences between the HOOP bands (position and bandwidths) in BR6.9 and K6.9 reflect differences in the degree of out-of-plane motion leading to a distortion of the retinal chromophore. A similar difference in HOOP motion is observed in the native K-590 spectra.[12] The absence of a shift in the position of the 1017-cm^{-1} band (C−CH_3 in-plane rocking mode) for BR6.9 and K6.9 indicates that the interaction between the CH_3 group and the adjacent amino acid(s) remains unchanged. Because the six-membered ring replaces the C_{19}−CH_3 group in BR6.9 (Figure 1), the 1017-cm^{-1} band can be assigned only to the rocking mode at the C_{20} position, *vide supra*. This conclusion is consistent with the C−CH_3 rocking data found in the photoreactions of native BR-570,[12] BR5.12,[17] and BR6.11.[32]

The kinetic parameters describing the intensity changes in these PTR/CARS features assigned to K6.9 correlate well with those obtained from PTA data (Figure 4), thereby demonstrating that K6.9 has separate, well-defined vibrational degrees of freedom.

C. Structure of Dark-Adapted BR6.9. Although it has been well-established that exposure of retinal-containing proteins to visible light at room temperature initiates structural changes involving both the retinal chromophore and its interactions with the surrounding protein environment,[1,36] it is useful to recall that two types of light-induced reactions are known: (i) a thermally reversible process between two stable (ground electronic state) BR species known as light- and dark-adapted BR and (ii) a photochemical process involving numerous intermediates (completed within ∼5 ms at room temperature) known as the BR photocycle. The thermal conversion of light-adapted BR (BR-570) to a mixture containing an approximately equal amount of dark-adapted BR (BR-548) occurs when the sample is placed in the dark for about 20 min at room temperature and pH 7. The shift in equilibrium concentrations between BR-570 and BR-548 is routinely detected by changes in absorption spectra.[36] Essentially total conversion of the dark-adapted mixture to BR-570 at room temperature occurs within a few seconds when the dark-adapted sample is exposed to visible light. The initial species in the native BR photocycle is light-adapted BR-570.[1,36]

Because retinal isomerization (all-*trans* to 13-*cis*) is thought to occur in both the dark adaptation and the photocycle of native BR,[36−38] the retinal chromophores in both BR-548 and the K-590 photocycle intermediate (formed in ∼3 ps from BR-570[8,9]) are assigned a 13-*cis* configuration.[12,37,38] Comparisons of the respective vibrational spectra of BR-548 and K-590, however, show each to have distinct retinal structures (and each distinct from that of BR-570[37,38]). Thus, if the retinal structures in BR-548 and K-590 are generally 13-*cis*-like, each has structural properties that differentiate one from the other (e.g., a difference in the C═N retinal configuration[36]).

The all-*trans* retinal in light-adapted BR6.9 also undergoes dark adaptation to form a 1:1 mixture of all-*trans* and 13-*cis* isomers[35]). Although this isomerization is not reflected in the respective absorption spectra, it is evident in the respective vibrational CARS spectra in which distinct C−C stretching bands appear (Figures 5 and 6).[11,12] On the basis of the observation that the dark-adapted BR6.9 mixture contains ∼50% 13-*cis* retinal (BR6.9/DA),[35] the differences in the C−C stretching bands establish that C_{13}═C_{14} isomerization occurs during the thermal dark adaptation of BR6.9. The absence of changes in the C−C stretching bands assignable to K6.9

indicates that, although structurally feasible, C_{13}═C_{14} isomerization does not occur in the photolytic formation of K6.9

Concluding Remarks

These PR/CARS results, together with previously published vibrational spectra from BR proteins,[6−12,17−20,25,33] lead to important, and unexpected, conclusions concerning the mechanistic role of C═C (and specifically C_{13}═C_{14}) isomerization in the BR6.9 photocycle. Analogous conclusions can be reached for the photocycles of other artificial BR pigments, extending perhaps even to the native BR photocycle itself.

PTR/CARS data (Figures 5 and 6) demonstrate that K6.9 contains a retinal with a structure that differs with respect to a variety of vibrational degrees of freedom (e.g., twisted retinal polyene chain and altered electron delocalization) from that in BR6.9. Because the C−C stretching features do not change between BR6.9 and K6.9 (Figure 5), however, the C═C bonding is not one of the differences and, therefore, there is no evidence that any C═C isomerization, including C_{13}═C_{14} isomerization, occurs as K6.9 is formed. Independently, the retinal configurations in both BR6.9, and most likely K6.9, can be determined to be all-*trans*-like on the basis of (i) the view that BR-570 contains an all-*trans* retinal[6−12,17−20,25,33] and (ii) the observation that the C−C stretching bands for BR-570, BR6.9, and K6.9 are similar (Table 1).

Analogously, the differences between the C−C stretching bands assigned to BR6.9 and BR6.9/DA (Figure 5), known to have respectively all-*trans*[7−10,33] and 13-*cis* retinals[35] show that C_{13}═C_{14} isomerization in BR6.9 can be monitored via vibrational spectroscopy. It is also important to note, however, that these C−C stretching bands in BR6.9/DA differ from those identifying C_{13}═C_{14} isomerization in 13-*cis* native K-590 (near 1196 cm^{-1}).[11,12] These differences in vibrational spectra assignable to a 13-*cis* retinal, already recognized in the vibrational spectra of BR-570 and BR-548,[11,12] emphasize the limitations of normal mode assignments in a system as complex as BR. Such results make it evident that vibrational spectra from BR proteins with retinal chromophores containing isotopes selectively introduced at specific bonds are needed to refine normal mode assignments and to expand their interpretations in terms of molecular structures.

Mechanistically, these results suggest that the general role of C_{13}═C_{14} isomerization as a primary structural event in BR photoreaction required for biochemical activity should be reexamined. In the native BR photocycle, C_{13}═C_{14} isomerization occurs as K-590 is formed,[11,12] and therefore, it is viewed as a fundamental structural event necessary for biochemical activity in the protein. Because PTR/CARS data presented here show that no C═C (C_{13}═C_{14}) isomerization is needed to form K6.9, even though BR6.9 exhibits biochemical activity[35] and the structure of BR6.9 permits C═C (C_{13}═C_{14}) isomerization (as in the thermal isomerization to form BR6.9/DA), it is evident that the biochemical mechanism in BR6.9, unlike native BR, proceeds with a K-intermediate that can undergo (C_{13}═C_{14}) isomerization, but does not. It is possible, of course, that C═C isomerization (either at the C_{13}═C_{14} bond or at another C═C bond) occurs later in the BR6.9 photocycle, but this proposal would have to be reconciled with the absence of absorption changes assignable to such an isomerization normally found to accompany structural changes in the retinal. Nonetheless, such an option needs to be examined via time-resolved vibrational spectroscopy measured over longer time scales.

Finally, the limitations associated with normal mode assignments to features in vibrational spectra as complex as those from BR proteins need to be recognized, especially when highly coupled normal modes are involved and specific structural properties are sought from the associated interpretations. In general, vibrational normal mode assignments in the BR photocycle intermediates need to be determined directly from vibrational spectra of both native and artificial samples containing retinals in which isotopes have been selectively introduced at specific retinal bonds. The high signal-to-noise ratios now available in vibrational CARS spectra justify such normal-mode analyses. In the absence of this type of experimental data and the associated assignments, the vibrational CARS spectra presented here cannot completely eliminate the possibility that retinal in K6.9 has isomerized relative to BR6.9 and specifically that C_{13}═C_{14} isomerization is required for biochemical functionality even in the BR6.9 photocycle. Obtaining such a more detailed, and potentially more accurate, understanding of the structural changes comprising the photoinduced biochemistry of retinal-containing proteins remains an important and challenging issue for future research.

Acknowledgment. The authors gratefully acknowledge Doug Hartz for technical assistance in the preparation of BR pigments. L.U. thanks Innovative Lasers Corp. for financial support. M.S. thanks the A.M.N. fund for the Promotion of Science, Culture, and Arts in Israel for generous support.

References and Notes

(1) Oesterhelt, D.; Tittor, J. *TIBS* **1989**, *14*, 57−61.
(2) Mathies, R. A.; Lin, S. W.; Ames, J. B.; Pollard, W. T. *Annu. Rev. Biophys. Biophys. Chem.* **1991**, *20*, 491−518.
(3) Lanyi, J. K. *FEBS Lett.* **1999**, *464* 103−107
(4) Lanyi, J. K. *Nature* **1995**, *375*, 461−463.
(5) Maeda, A. *Isr. J. Chem.* **1995**, *35*, 387−400.
(6) Stoeckenius, W. *Protein Sci.* **1999**, *8*, 447−459.
(7) Atkinson, G. H.; Ujj, L.; Zhou, Y. *J. Phys. Chem. A* **2000**, *104*, 4130−4139.
(8) Smith, S. O. Ph.D. Dissertation, University of California, Berkeley, CA, 1985; pp 1−344.
(9) Smith, S. O.; Braiman, M.; Myers, A. B.; Pardoen, J. A.; Courtin, J. M.; Winkel, C. Lugtenburg, J.; Mathies, R. A. *J. Am. Chem. Soc.* **1987**, *109*, 3108−3125.
(10) Smith, S. O.; Pardoen, J. A.; Lugtenburg, J.; Mathies, R. A. *J. Phys. Chem.* **1987**, *91*, 804−819.
(11) Brack, T. L.; Atkinson, G. H. *J. Mol. Struct.* **1989**, *214*, 289−303.
(12) Ujj, L.; Jäger, F.; Popp, A.; Atkinson, G. H. *Chem. Phys.* **1996**, *212*, 421−436.
(13) Ye, T.; Friedman, N.; Gat, Y.; Atkinson, G. H.; Sheves, M.; Ottolenghi, M.; Ruhman, S. J. *J. Phys. Chem. B* **1999**, *103*, 5122−5130.
(14) Rousso, I.; Khachatyran, E.; Gat, Y.; Brodsky, I.; Ottolenghi, M.; Sheves, M.; Lewis, A. *Proc. Natl. Acad. Sci. U.S.A.* **1997**, *94*, 7937−7941.
(15) Rousso, I.; Gat, Y.; Lewis, A.; Sheves, M.; Ottolenghi, M. *Biophys. J.* **1998**, *75*, 413−417.
(16) Aharoni, A.; Weiner, I.; Ottolenghi, M.; Sheves, M. *J. Biol. Chem.* **2000**, *275*, 21010−21016.
(17) Ujj, L.; Zhou, Y.; Sheves, M.; Ottolenghi, M.; Atkinson, G. H. *J. Am. Chem. Soc.* **2000**, *122*, 96−106.
(18) Delaney, J. K.; Atkinson, G. H.; Sheves, M.; Ottolenghi, M. *J. Phys. Chem.* **1995**, *99*, 7801−7805.
(19) Petrich, J. W.; Breton, J.; Martin, J. L.; Antonetti, A. *Chem. Phys. Lett.* **1987**, *137*, 369−375.
(20) Doig, S. J.; Reid, P. J.; Mathies, R. A. *Biomol. Spectrosc.* **1991**, *1432*, 184−195.
(21) Song, L.; El-Sayed, M. A. *J. Am. Chem. Soc.* **1999**, *120*, 8889−8890.
(22) Hasson, K. C.; Gai, F.; Anfinrud, P. A. *Proc. Natl. Acad. Sci. U.S.A.* **1996**, *93*, 15124−15129.
(23) Callender, R. H.; Honig, B. *Annu. Rev. Biophys. Bioeng.* **1977**, *6*, 33−55.
(24) Birge, R. R.; Findsen, L. A.; Pierce, B. M. *J. Am. Chem. Soc.* **1987**, *109*, 5041−5043.
(25) Weidlich, O.; Ujj, L.; Jäger, F.; Atkinson, G. H. *Biophys. J.* **1997**, *72*, 2329−2341.
(26) Ujj, L.; Jäger, F.; Popp, A.; Atkinson, G. H. *Chem. Phys.* **1996**, *212*, 421−436.

(27) Lohrmann, R.; Grieger, I.; Stockburger, M. *J. Phys. Chem.* **1991**, *95*, 1993−2001.

(28) Lohrmann, R.; Stockburger, M., *J. Raman Spectrosc.* **1992**, *23*, 575−583.

(29) Oesterhelt, D.; Stoeckenius, W. *Proc. Natl. Acad. Sci. U.S.A.* **1973**, *70*, 2853−2857.

(30) Ujj, L.; Jäger, F.; Atkinson, G. H. *Biophys. J.* **1998**, *74*, 1492−1501.

(31) Ujj, L.; Volodin, B. L.; Popp, A.; Delaney, J. K.; Atkinson, G. H. *Chem. Phys.* **1994**, *182*, 291−311.

(32) Ujj, L.; Zhou, Y.; Atkinson, G. H., to be submitted for publication.

(33) Doig, S. J.; Reid, P. J.; Mathies, R. A. *J. Phys. Chem.* **1991**, *95*, 6372−6379.

(34) Albeck, A.; Friedman, N.; Sheves, M.; Ottolenghi, M. *J. Am. Chem. Soc.* **1986**, *108*, 4614−4618.

(35) Schrader, B.; Meier, W. *DMS Raman/IR Atlas*; Verlag Chemie, GmbH: Weinheim, Germany, 1975; Vol. 1.

(36) Birge, R. R. *Biochim. Biophys. Acta* **1990**, *1016*, 293−327.

(37) Nonella, M.; Windemuth, A.; Schulten, K. *Photochem. Photobiol.* **1991**, *54*, 937−948.

(38) Harbison, G. S.; Smith, S. O.; Pardoen, J. A.; Winkel, C.; Lugtenburg, J.; Herzfeld, J.; Mathies, R.; Griffin, R. G. *Proc. Natl. Acad. Sci. U.S.A.* **1984**, *81*, 1706−1709.